CrystEngComm

RSC Publishing

PAPER

View Article Online
View Journal | View Issue

New insights into the BiB_3O_6 melt structure†

Yulong Sun,[a] Songming Wan,*[a] Xianshun Lv,[a] Xiaolu Tang,[a] Jinglin You[b] and Shaotang Yin[a]

Cite this: *CrystEngComm*, 2013, **15**, 995

The structure of borate melt has long been a fundamental unsolved problem in condensed matter physics, materials chemistry. Here, we use high temperature Raman spectroscopy and first principles calculations to study the structural change before and after the melting of a BiB_3O_6 crystal to obtain the BiB_3O_6 melt structure. A transformation of the 4-fold coordinated boron atoms to 3-fold coordinated boron atoms and a destruction of the atomic configuration around the Bi^{3+} ions were found when the crystal melted. Considering the growth habit of the BIBO crystal, we proposed a polymer model for the first time to describe the melt structure. The BiB_3O_6 melt is made up of special $[B_3O_3Ø_3]$ (Ø = bridging oxygen) structural units, which further polymerize into $[B_3O_3Ø_3]_n$ chains by sharing oxygen atoms; the boron–oxygen chains are surrounded by the Bi^{3+} ions. Density functional theory (DFT) calculations were carried out to simulate the melt Raman spectrum based on the structural unit. The calculated BiB_3O_6 melt Raman spectrum shows good agreement with the experimental spectrum. The main vibrational bands were assigned. The strongest band below 400 cm^{-1} is mainly attributed to the wagging vibration of the side $BØO_2$ triangle as a whole; the band located around 630 cm^{-1} is assigned to the bending vibrations of the $[B_3O_3Ø_3]_n$ chain; the bands in the range of 1200–1500 cm^{-1} arise from the stretching vibrations of B–O (or B–Ø) bonds in the boron–oxygen triangles.

Received 23rd October 2012,
Accepted 15th November 2012

DOI: 10.1039/c2ce26742j

www.rsc.org/crystengcomm

1 Introduction

Fast development in laser medicine, full color display, optical communication and signal processing has created increasing demands for highly efficient and compact all-solid-state lasers used in the visible and ultraviolet regions. An effective approach to generate such lasers is by frequency conversion of solid-state lasers using nonlinear optical (NLO) crystals.[1,2] The α-BiB_3O_6 (BIBO) crystal is an outstanding NLO material. Its effective NLO coefficient along the phase matching direction is 3.2 pm V^{-1}, larger than that of the widely used NLO crystals, such as $KTiOPO_4$, β-BaB_2O_4, and LiB_3O_5. The crystal also possesses a wide transparency range (280–2500 nm), a high damage threshold (300 MW cm^{-2}) and a large angular acceptance (2.7 mrad cm^{-1}).[3–5] Third harmonic picosecond laser (355 nm) and tunable femtosecond lasers from 375 nm to 435 nm have also been achieved by using the crystal.[6,7]

BIBO crystals have been grown from the stoichiometric BiB_3O_6 melt by top-seeded method.[8–10] During the past two decades, substantial efforts have been put into the crystal growth. However, the goal of reproducible growth of high-quality BIBO crystals is far from being achieved. One problem is the very high viscosity of the BiB_3O_6 melt, which limits mass transport, inhibits initial nucleation, and leads to a very low growth rate.[8] Another problem is a metastable eutectic mixture, $Bi_3B_5O_{12}$ and α-$Bi_2B_8O_{15}$, often present in the crystal growth process.[11] Besides, the phase relationships of the BiB_3O_6 system are very complicated. So far four different polymorphs, monoclinic α-BiB_3O_6,[12] β-BiB_3O_6,[13] γ-BiB_3O_6[13] and orthorhombic δ-BiB_3O_6,[14] have been reported. α-BiB_3O_6 is stable only in a narrow temperature range near the melting point.[15]

The BiB_3O_6 melt structure, in particular that near the melting point, provides a basis for deeply understanding the thermodynamic properties of the melt and the phase relationships in the BiB_3O_6 system.[16–18] On one hand, the BiB_3O_6 melt structure is a major factor determining the macroscopic properties, such as viscosity, density and surface tension. On the other hand, the BiB_3O_6 melt structure is associated to the structures of the equilibrium BiB_3O_6 crystals. The characteristics of the BiB_3O_6 melt structure can pass down to BiB_3O_6 crystals and impact their structures (phase relationships), growth habits and qualities.

However, the structure of the borate melt has long been a fundamental unsolved problem in condensed matter physics, materials chemistry.[17] Borate glass is widely used as the analogue for the structural study of the corresponding melt,

[a]*Anhui Key Laboratory for Photonic Devices and Materials, Anhui Institute of Optics and Fine Mechanics, Chinese Academy of Sciences, Hefei 230031, China. E-mail: smwan@aiofm.ac.cn; Fax: +86 0551 5591054; Tel: +86 0551 5591054*
[b]*School of Material Science and Engineering, Shanghai University, Shanghai 200072, China*

† Electronic supplementary information (ESI) available: Geometrical parameters of the optimized melt structural unit. See DOI: 10.1039/c2ce26742j

which avoids the experimental difficulties under high-temperature conditions. However, this method is still debatable because the glass structure represents the structure of the supercooled melt at the glass transition temperature rather than that of the high-temperature melt.[17] Accurate description of a melt structure requires high-temperature *in-situ* experimental technologies. Raman and infrared spectroscopy,[19,20] nuclear magnetic resonance,[21] X-ray diffraction,[22] and neutron diffraction[23] are the popular *in-situ* techniques to study melt structures. Compared with the other techniques, Raman spectroscopy is a powerful and convenient tool for the study of melt structures.[19,24–31] However, the conversion of the vibrational peaks seen in the Raman spectrum into structural information remains difficult. Raman peaks of borate melts are usually assigned by comparison with the spectra of crystalline compounds based on the assumption proposed by Krogh–Moe that the structural units present in melts resemble those present in the crystalline compounds.[32] As we know, boron combines with oxygen not only in triangular but also in tetrahedral coordination, the triangular and the tetrahedral boron–oxygen units may further polymerize by sharing oxygen atoms and give rise to great structural diversity. The structural diversity often makes reliable assignments of Raman vibrational peaks difficult. The situation will be more complicated when more than one unit gives rise to Raman peaks in the same region or when the borate compound contains two or more units.

Recently, density functional theory (DFT) has been used to predict and interpret Raman spectra for a wide range of materials, including crystalline solids,[33] polymers[34] and molecules.[35] Good agreement between the experimental and the calculated Raman spectra has been achieved; reliable assignments of all experimental Raman peaks can be provided. Here, we investigate the BiB_3O_6 melt structure near the melting point with high-temperature Raman spectroscopy. DFT calculations are carried out to interpret the crystal and melt Raman spectra and to extract their structural information. This study will give a novel polymer model to describe the melt structure.

2 Experimental section

Unpolarized Raman spectra of the BIBO crystal and BiB_3O_6 melt were recorded on a Jobin Y'von U1000 laser Raman spectrometer with the 532 nm line of a Q-switch pulsed SHG-Nd:YAG laser as the excitation source. The Raman scattering light from the samples was collected by a back-scattering confocal lens system, and detected by an intensive charge-coupled device (ICCD). The spectral acquisition, under accumulated mode, was 10 s each time with 10 repetition times. The average laser power was fixed at 0.8 W. Raman spectra in the range of 200–1800 cm^{-1} were recorded with the spectral resolution better than 2 cm^{-1}.

The homemade micro-furnace used in this work has been described previously.[36] A BIBO crystal slice with a size of 5 × 10 × 20 mm^3 was placed in a platinum boat, and then into the micro-furnace with the boat. The micro-furnace provided a horizontal temperature gradient in the boat. By carefully controlling the temperature, a steady crystal–melt interface was produced. The melt Raman spectra, as well as the crystal Raman spectra, were collected near the crystal–melt interface in order to ensure the measuring temperature close to the melting point.

All DFT calculations were carried out by the plane-wave pseudopotential method implemented in the CASTEP (Cambridge Sequential Total Energy Package) code.[37] The PBE (Perdew–Burke–Ernzerhof) version of the GGA (generalized gradient approximation) was used in conjunction with norm-conserving pseudopotentials, the cutoff energy was set to 750 eV. The experimentally determined BIBO crystal structure was adopted as the initial structure for geometrical optimization;[12] the melt structure was constructed according to the spectral analysis results, as shown in the Results and discussion section. The geometrical optimization was done with the SCF (self-consistent field) convergence criterion of 1 × 10^{-8} eV $atom^{-1}$. Brillouin zone sampling of electronic states was performed on a 4 × 6 × 4 Monkhorst–Pack *k*-point grid for the crystal and on a 4 × 2 × 3 grid for the melt.[38] Density functional perturbation theory (DFPT)[39] calculations were carried out to compute the dynamical matrices, which were diagonalized to give Raman frequencies. Raman activities were computed by a hybrid method combining DFPT with the finite displacement method.[40] In order to obtain the Raman scattering intensities, the Raman activities were multiplied by Bose–Einstein factors corresponding to the experimental temperatures and the excitation source wavelength (532 nm).[41] The CASTEP outputs include the Raman frequencies and intensities of all Raman-active vibrational modes, as well as the atomic displacements for each mode.

3 Results and discussion

The room temperature Raman spectrum of the BIBO crystal is shown in Fig. 1. With temperature increasing, no significant

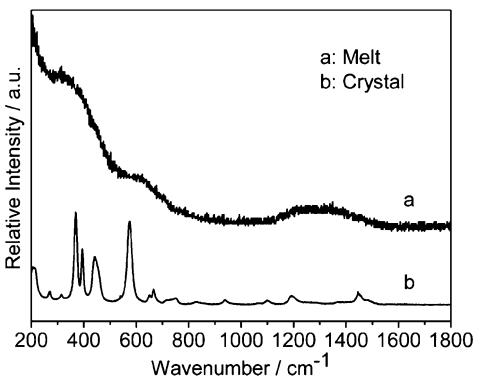

Fig. 1 Raman spectra of BIBO crystal (at room temperature) and BiB_3O_6 melt (at the melting point).

change was observed in the spectrum except for peaks broadening and slight frequency red-shift, as reported in our previous work.[42] However, the spectrum changed remarkably when the crystal melted. The BiB_3O_6 melt spectrum has three strong Raman vibrational bands located around 370 cm^{-1}, 630 cm^{-1} and in the range of 1200–1500 cm^{-1}. As compared to the crystal spectrum, the relative intensity of the Raman band in the 1200–1500 cm^{-1} region increases; the strong crystal peak located at 574 cm^{-1} disappears.

As the BIBO crystal structure has been determined, if we gain the structural evolution information during the melting process, the BiB_3O_6 melt structure will be derived. In this work, the structural evolution is reflected by the Raman spectral changes before and after the melting of the BIBO crystal. In order to understand the structural origins of the spectral changes, some important Raman peaks both of the crystal and of the melt should be clearly assigned.

Hu *et al.* reported the Raman spectrum of the BIBO crystal and assigned all the Raman vibrational peaks.[43] Due to the structural complexity of the crystal, the internal vibrational peaks were approximately attributed to the vibrations of BO_4 tetrahedra or BO_3 triangles although the two groups are not independent in the crystal structure. In this paper, we calculate the Raman spectrum of BIBO crystal by DFT method and give clearer assignments of some important crystal Raman peaks.

The calculated Raman spectrum is shown in Fig. 2, along with the experimental spectrum. All calculated frequencies, except 390 cm^{-1} and 625 cm^{-1}, coincide well with the experimental values within an acceptable error (15 cm^{-1}). The relative intensities of all calculated peaks, except that of 390 cm^{-1} peak, are also consistent with the experimental results. According to the calculated results, the crystal peaks in the high frequency region (1200–1500 cm^{-1}) are mainly associated with the stretching vibrations of B–Ø bonds (B_3–Ø) in $BØ_3$ groups (see Fig. 3(c) and 3(d)). When the crystal melted, the relative intensity of the high frequency band increased, as shown in Fig. 1, implying the number of the B_3–Ø bonds increased. We deem that the increase originates from the conversion of 4-fold coordinated boron atoms to 3-fold coordinated boron atoms. During the melting process, one B–Ø bond (B_4–Ø) in a $BØ_4$ group broke to form a new $BØ_3$ group. The conversion has been found in various borate melts[25,44–46] and is also supported by the spectral characteristics of the BiB_3O_6 melt in the range of 800–1100 cm^{-1}. The strong Raman peaks in this range are related to the asymmetric stretching vibrations of $BØ_4$ tetrahedra (the atomic displacements corresponding to the calculated 934 cm^{-1} peak is visualized in Fig. 3 (b)). In the BiB_3O_6 melt Raman spectrum, no obvious Raman peaks are present in the range, indicating no $BØ_4$ tetrahedra present in the melt. The experimental 574 cm^{-1} peak (corresponding to the calculated 561 cm^{-1} peak) arises from the Bi–Ø symmetric stretching vibration of the $BiØ_4$ pyramids in the BIBO crystal structure (see Fig. 3 (a)). The disappearance of the peak reflects that the pyramids were destroyed when the crystal melted.

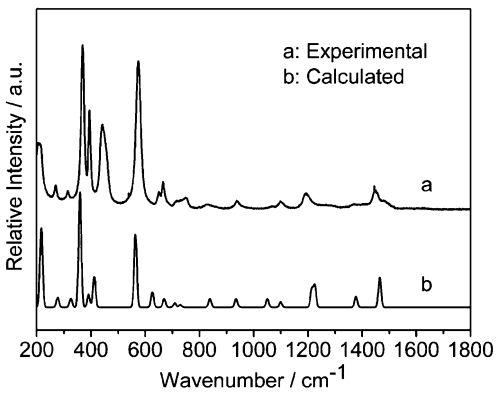

Fig. 2 Experimental and calculated Raman spectra of the BIBO crystal.

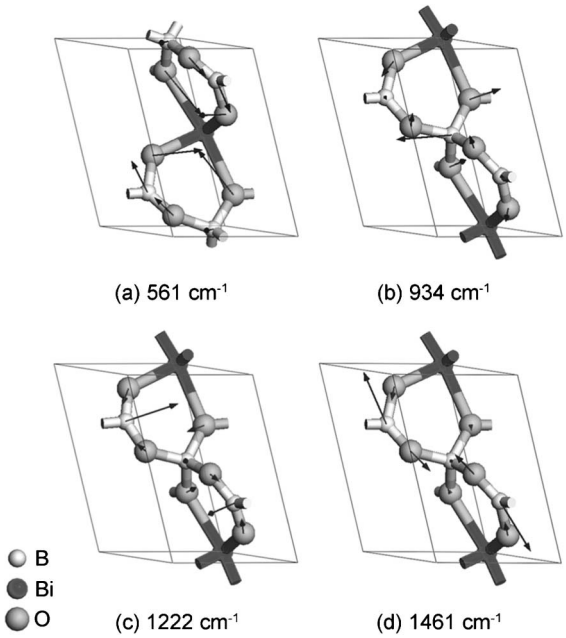

Fig. 3 Graphic representations of the atomic displacements of the calculated peaks at 561 cm^{-1}, 934 cm^{-1}, 1222 cm^{-1} and 1464 cm^{-1}.

The growth habit of the BIBO crystal also supports the above analysis. In general, crystal morphology is dominated by the slow-growing faces. According to the attachment energy model for crystal growth habit, the relative growth rate of a face is assumed to be proportional to its attachment energy, which is defined as the bond energy released when one additional growth slice of thickness d_{hkl} is attached to the crystal face identified by the Miller indices *hkl*.[47] Therefore, the faces with small attachment energy, *viz.* the faces connected with weak bonds, will present in the final crystal morphology. Becker *et al.* found that the {110}, {111}, {102} and {001} faces dominate the final morphology of the BIBO crystal.[8] According to the crystal structure, the {110}, {111} and {102} faces are all connected with B_4–Ø bonds and the {001} faces are connected with Bi–Ø bands (see Fig. 4). Thus, we can

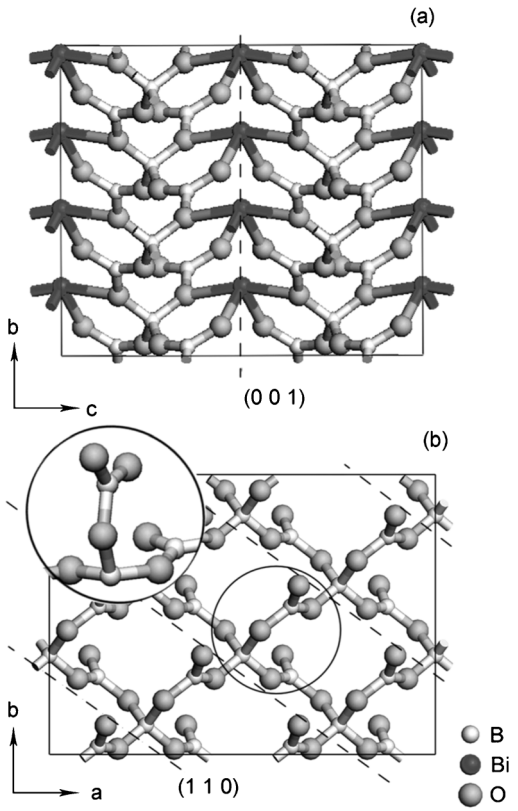

Fig. 4 BIBO crystal structure: (a) the projection as viewed along the *a* axis; (b) the projection as viewed along the *c* axis (without Bi^{3+} ions).

conclude that both of the B_4–Ø bonds and the Bi–Ø bonds are the weak bonds in the BIBO crystal structure and likely to break when the crystal melts.

Based on the structural evolution from the BIBO crystal to the BiB_3O_6 melt (see Fig. 4), we proposed a boron–oxygen structural model to describe the BiB_3O_6 melt. Here, we take the case of the (110) and (001) faces as the example. When the Bi–Ø bonds break along the (001) face, two-dimensional boron–oxygen networks form. The two-dimensional networks further decompose into polymer-like boron–oxygen chains when the B_4–Ø bonds break along the (110) face. The chain has a *meta*-borate chain-type backbone, in which every other non-bridging boron atom is substituted by a $BO_2Ø$ triangle to form a $[B_3O_3Ø_3]_n$ chain. We deem that the BiB_3O_6 melt is made up of special $[B_3O_3Ø_3]_n$ chains.

Based on the structural model proposed for the BiB_3O_6 melt, we have calculated the melt Raman spectrum. It is well known that CASTEP calculations must be performed in a three-dimensional periodic system.[37] In order to satisfy the condition, a periodic supercell method is often used for the CASTEP calculations of chain-type polymers.[40] The chain is artificially repeated in two dimensions normal to the chain direction, the unit cell sizes along the two dimensions are sufficiently large so as to make the neighboring interactions negligible. For example, Zeng *et al.* have used this supercell method to study the lattice dynamics of polyaniline and

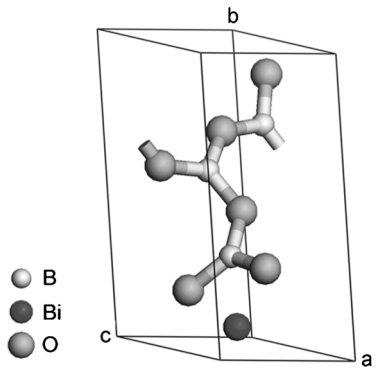

Fig. 5 The optimized structure of the fundamental unit in the BiB_3O_6 melt.

poly(*p*-pyridyl vinyline).[34] Here, we use a similar method to calculate the BiB_3O_6 melt Raman spectrum. The fundamental melt structural unit $[B_3O_3Ø_3]$, as shown in Fig. 4, was placed into a unit cell with the chain along the *c* axis, a Bi^{3+} ion was added in the vicinity of the three non-bridging oxygen atoms for charge compensation. Considering the strong electrostatic interactions between the chains, between the chains and the Bi^{3+} ions, and between the Bi^{3+} ions, we did not limit the unit cell parameters and the atomic positions during the DFT geometry optimization. The melt Raman spectrum was simulated at the same level of theory as was used for the crystal calculations besides the *k*-point set (see the experimental section for more details).

The optimized geometric structure of the fundamental structural unit is shown in Fig. 5. The B–O bond lengths (1.35–1.40 Å) and the O–B–O bond angles (115°–125°) coincide with the reported values of boron–oxygen triangles (see the ESI† for more details). The calculated Raman spectrum is presented in Fig. 6. All Raman intensities were corrected by Bose–Einstein factors with the temperature of 1000 K (the melting point of

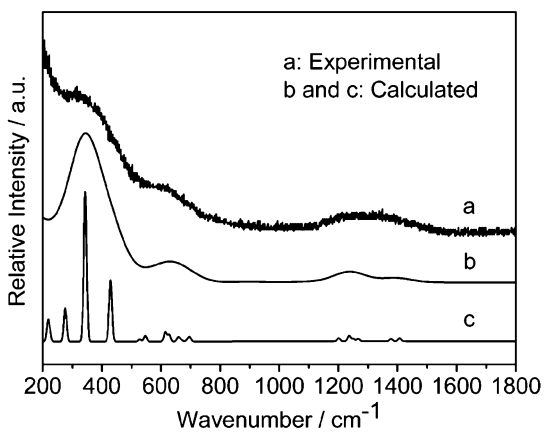

Fig. 6 The experimental and calculated Raman spectra of the BiB_3O_6 melt. (a) The experimental Raman spectrum. (b) The calculated Raman spectrum broadened by Gaussian line shape function with a FWHM of 50 cm^{-1}. (c) The calculated Raman spectrum broadened by Gaussian line shape function with a FWHM of 5 cm^{-1}.

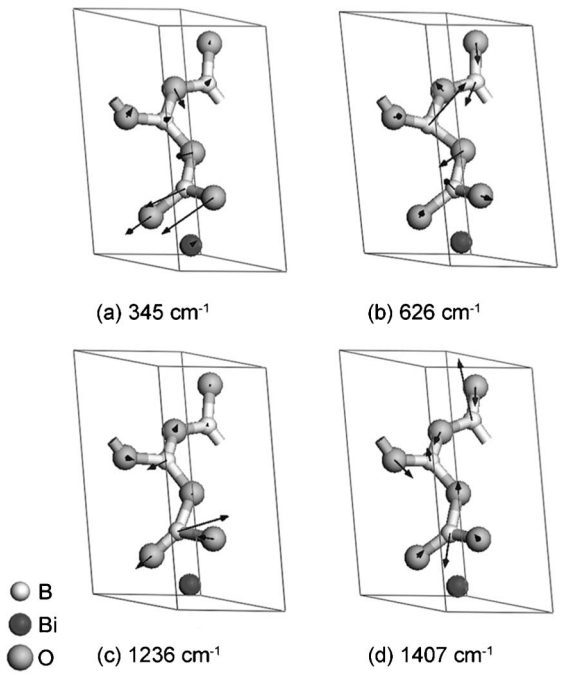

Fig. 7 Atomic displacements of four main peaks in the calculated Raman spectrum.

the BIBO crystal) and the wavelength of 532 nm (the wavelength of the excitation source). The temperature dependence (thermal broadening) of the Raman peak shape was simulated by a Gaussian line shape function with a FWHM (full width at half maximum) of 50 cm^{-1}.[24,28] The superposition of these Gaussian profiles is shown in Fig. 6(b), which is in good agreement with the experimental melt spectrum. The intense Raman scattering signal in the low-frequency region of the experimental spectrum is attributed to the background thermal radiation of the melt.[48]

Fig. 7 gives the atomic displacements of the important vibrational modes that are responsible for the strong Raman bands in the melt spectrum. The strong band below 400 cm^{-1} is mainly attributed to the wagging vibration of the side $BO_2Ø$ triangle as a whole (see Fig. 7(a)). The band centered at 630 cm^{-1} is associated with the bending vibrations of the $[B_3O_3Ø_3]_n$ chain (see Fig. 7(b)). The vibrational band in the range of 1200–1500 cm^{-1} contains two sub-bands, located around 1240 cm^{-1} and 1410 cm^{-1}. Both the sub-bands are attributed to the stretching vibrations of the B_3–O (or B_3–Ø) bonds (see Fig. 7(c) and 7(d)).

4 Conclusions

A Raman spectrum investigation on the BiB_3O_6 melt has been undertaken assisted with DFT calculations. Some important BIBO crystal Raman peaks have been assigned: (1) the peaks in the high frequency region (1200–1500 cm^{-1}) are associated with the stretching vibration of the B_3–Ø bonds. (2) The strong 574 cm^{-1} peak arises from the symmetric stretching vibration of the $BiØ_4$ pyramids. When the crystal melted, the relative intensity of the Raman bands in the range of 1200–1500 cm^{-1} increased and the 574 cm^{-1} peak disappeared. The spectral changes are due to the conversion of the 4-fold coordinated boron atoms to 3-fold coordinated boron atoms and the destruction of the atomic configuration around the Bi^{3+} ions. Based on the structural changes, we proposed a polymer model to describe the BiB_3O_6 melt structure. The BiB_3O_6 melt is made up of $[B_3O_3Ø_3]$ structural units, which polymerize into special $[B_3O_3Ø_3]_n$ chains by sharing oxygen atoms; the boron–oxygen chains are surrounded by Bi^{3+} ions. DFT calculations verified the melt structure and provided clear assignments of the strong peaks in the melt Raman spectrum. The strongest band below 400 cm^{-1} is mainly attributed to the wagging vibration of the side $BO_2Ø$ triangle as a whole; the band centered around 630 cm^{-1} is associated with the bending vibrations of the chain; the vibrational bands in the range of 1200–1500 cm^{-1} are assigned to the stretching vibrations of the B_3–O (or B_3–Ø) bonds.

Our work demonstrates that DFT calculations are reliable methods to establish valuable links between Raman spectral features and structural information not only of a crystal but also a melt. The polymer model provides us a new viewpoint on the borate melt structure and is expected to help us deeply understand the thermodynamic properties of the BiB_3O_6 melt and the phase relationships in the BiB_3O_6 system.

Acknowledgements

This work is financially supported by the National Natural Science Foundation of China (grant no. 50932005) and Open Research Program of Key Laboratory of Functional Crystals and Laser Technology, Technical Institute of Physics and Chemistry, Chinese Academy of Sciences.

References

1 T. Sasaki, Y. Mori, M. Yoshimura, Y. K. Yap and T. Kamimura, *Mater. Sci. Eng., R*, 2000, **30**, 1–54.
2 P. Becker, *Adv. Mater.*, 1998, **10**, 979–992.
3 H. Hellwig, J. Liebertz and L. Bohaty, *Solid State Commun.*, 1998, **109**, 249–251.
4 H. Hellwig, J. Liebertz and L. Bohaty, *J. Appl. Phys.*, 2000, **88**, 240–244.
5 M. Ghotbi and M. Ebrahim-Zadeh, *Opt. Express*, 2004, **12**, 6002–6019.
6 M. Ghotbi, Z. Sun, A. Majchrowski, E. Michalski, I. V. Kityk and M. Ebrahim-Zadeh, *Appl. Phys. Lett.*, 2006, **89**, 173124.
7 M. Ghotbi, M. Ebrahim-Zadeh, A. Majchrowski, E. Michalski and I. V. Kityk, *Opt. Lett.*, 2004, **29**, 2530–2532.
8 P. Becker, J. Liebertz and L. Bohaty, *J. Cryst. Growth*, 1999, **203**, 149–155.
9 B. Teng, J. Y. Wang, Z. P. Wang, X. B. Hu, H. D. Jiang, H. Liu, X. F. Cheng, S. M. Dong, Y. G. Liu and Z. S. Shao, *J. Cryst. Growth*, 2001, **233**, 282–286.

10 B. Teng, J. Y. Wang, Z. P. Wang, H. D. Jiang, X. B. Hu, R. B. Song, H. Liu, Y. G. Liu, J. Q. Wei and Z. S. Shao, *J. Cryst. Growth*, 2001, **224**, 280–283.
11 F. Y. Zavartsev, S. A. Koutovoi, V. V. Voronov, V. V. Panyutin, A. I. Zagumennyi and I. A. Shcherbakov, *J. Cryst. Growth*, 2005, **275**, e637–e641.
12 R. Frohlich, L. Bohaty and J. Liebertz, *Acta Crystallogr., Sect. C: Cryst. Struct. Commun.*, 1984, **40**, 343–344.
13 L. Y. Li, G. B. Li, Y. X. Wang, F. H. Liao and J. H. Lin, *Inorg. Chem.*, 2005, **44**, 8243–8248.
14 J. S. Knyrim, P. Becker, D. Johrendt and H. Huppertz, *Angew. Chem., Int. Ed.*, 2006, **45**, 8239–8241.
15 R. H. Cong, J. L. Zhu, Y. X. Wang, T. Yang, F. H. Liao, C. Q. Jin and J. H. Lin, *CrystEngComm*, 2009, **11**, 1971–1978.
16 M. W. Schmidt, J. A. D. Connolly, D. Gunther and M. Bogaerts, *Science*, 2006, **312**, 1646–1650.
17 G. Calas, G. S. Henderson and J. F. Stebbins, *Elements*, 2006, **2**, 265–268.
18 V. Ginkin, A. Kartavykh and M. Zabudko, *J. Cryst. Growth*, 2004, **270**, 329–339.
19 T. Yano, S. Shibata and T. Maehara, *J. Am. Ceram. Soc.*, 2006, **89**, 89–95.
20 F. Domine and B. Piriou, *J. Non-Cryst. Solids*, 1983, **55**, 125–130.
21 S. Sen, Z. Xu and J. F. Stebbins, *J. Non-Cryst. Solids*, 1998, **226**, 29–40.
22 G. Herms and J. Sakowski, *Phys. Chem. Glasses*, 2000, **41**, 309–312.
23 T. Kordel, D. Holland-Moritz, F. Yang, J. Peters, T. Unruh, T. Hansen and A. Meyer, *Phys. Rev. B: Condens. Matter Mater. Phys.*, 2011, **83**, 104205.
24 T. Yano, N. Kunimine, S. Shibata and M. Yamane, *J. Non-Cryst. Solids*, 2003, **321**, 137–146.
25 T. Yano, N. Kunimine, S. Shibata and M. Yamane, *J. Non-Cryst. Solids*, 2003, **321**, 147–156.
26 T. Yano, N. Kunimine, S. Shibata and M. Yamane, *J. Non-Cryst. Solids*, 2003, **321**, 157–168.
27 Y. K. Voron'ko, A. A. Sobol' and V. E. Shukshin, *J. Mol. Struct.*, 2012, **1008**, 69–76.
28 A. A. Osipov and L. M. Osipova, *Phys. B*, 2010, **405**, 4718–4732.
29 A. A. Osipov and L. M. Osipova, *Phys. Chem. Glasses: Eur. J. Glass Sci. Technol., Part B*, 2009, **35**, 121–131.
30 A. A. Osipov and L. M. Osipova, *Phys. Chem. Glasses: Eur. J. Glass Sci. Technol., Part B*, 2009, **35**, 131–140.
31 L. M. Osipova, A. A. Osipov and V. N. Bykov, *Phys. Chem. Glasses: Eur. J. Glass Sci. Technol., Part B*, 2007, **33**, 486–491.
32 J. Krogh-Moe, *J. Non-Cryst. Solids*, 1969, **1**, 269–284.
33 V. Milman, A. Perlov, K. Refson, S. J. Clark, J. Gavartin and B. Winkler, *J. Phys.: Condens. Matter*, 2009, **21**, 485404.
34 G. Zheng, S. J. Clark, S. Brand and R. A. Abram, *Phys. Rev. B: Condens. Matter Mater. Phys.*, 2006, **74**, 165210.
35 T. T. Lin, X. Y. Liu and C. B. He, *J. Phys. Chem. B*, 2012, **116**, 1524–1535.
36 S. M. Wan, X. Zhang, S. J. Zhao, Q. L. Zhang, J. L. You, H. Chen, G. C. Zhang and S. T. Yin, *J. Appl. Crystallogr.*, 2007, **40**, 725–729.
37 M. D. Segall, J. D. L. dan Philip, M. J. Probert, C. J. Pickard, P. J. Hasnip, S. J. Clark and M. C. Payne, *J. Phys.: Condens. Matter*, 2002, **14**, 2717–2744.
38 H. J. Monkhorst and J. D. Pack, *Phys. Rev. B: Solid State*, 1976, **13**, 5188–5192.
39 K. Refson, P. R. Tulip and S. J. Clark, *Phys. Rev. B: Condens. Matter Mater. Phys.*, 2006, **73**, 155114.
40 V. Milman, K. Refson, S. J. Clark, C. J. Pickard, J. R. Yates, S. P. Gao, P. J. Hasnip, M. I. J. Probert, A. Perlov and M. D. Segall, *J. Mol. Struct. (THEOCHEM)*, 2010, **954**, 22–35.
41 R. Baddour-Hadjean, M. B. Smirnov, K. S. Smirnov, V. Y. Kazimirov, J. M. Gallardo-Amores, U. Amador, M. E. Arroyo-de Dompablo and J. P. Pereira-Ramos, *Inorg. Chem.*, 2012, **51**, 3194–3201.
42 S. M. Wan, B. Teng, X. Zhang, J. L. You, W. P. Zhou, Q. L. Zhang and S. T. Yin, *CrystEngComm*, 2010, **12**, 211–215.
43 X. B. Hu, J. Y. Wang, B. Teng, C. K. Loong and M. Grimsditch, *J. Appl. Phys.*, 2005, **97**, 033501.
44 S. M. Wan, X. Zhang, S. J. Zhao, Q. L. Zhang, J. L. You, L. Lu, P. Z. Fu, Y. C. Wu and S. T. Yin, *Cryst. Growth Des.*, 2008, **8**, 412–414.
45 R. Akagi, N. Ohtori and N. Umesaki, *J. Non-Cryst. Solids*, 2001, **293**, 471–476.
46 O. Majerus, L. Cormier, G. Calas and B. Beuneu, *J. Phys. Chem. B*, 2003, **107**, 13044–13050.
47 M. Brunsteiner, A. G. Jones, F. Pratola, S. L. Price and S. J. R. Simons, *Cryst. Growth Des.*, 2005, **5**, 3–16.
48 G. C. Jiang, J. L. You, B. K. Yu and S. P. Huang, *Spectrosc. Spectral Anal.*, 2000, **20**, 206–209.

